Virology 494 (2016) 236–247

Contents lists available at ScienceDirect

Virology

journal homepage: www.elsevier.com/locate/yviro

Viral genome imaging of hepatitis C virus to probe heterogeneous viral infection and responses to antiviral therapies

Vyas Ramanan [a,1], Kartik Trehan [a,1], Mei.-Lyn. Ong [b], Joseph M. Luna [c], Hans.-Heinrich Hoffmann [c], Christine Espiritu [c], Timothy P. Sheahan [c,2], Hamsika Chandrasekar [d], Robert E. Schwartz [a,3], Kathleen S. Christine [a], Charles M. Rice [c], Alexander van Oudenaarden [f,g,h], Sangeeta N. Bhatia [a,d,e,i,j,*]

[a] Institute for Medical Engineering and Science, Massachusetts Institute of Technology, Cambridge, MA 02139, USA
[b] Computational and Systems Biology, Massachusetts Institute of Technology, Cambridge, MA 02139, USA
[c] Center for the Study of Hepatitis C, Laboratory of Virology and Infectious Disease, The Rockefeller University, New York, 10065 NY, USA
[d] Department of Electrical Engineering and Computer Science, Massachusetts Institute of Technology, Cambridge, MA 02139, USA
[e] Division of Medicine, Brigham and Women's Hospital, Boston, MA 02115, USA
[f] Department of Physics, Massachusetts Institute of Technology, Cambridge, MA 02139, USA
[g] Department of Biology, Massachusetts Institute of Technology, Cambridge, MA 02139, USA
[h] Hubrecht Institute, Royal Netherlands Academy of Arts and Sciences, and University Medical Center Utrecht, Uppsalalaan 8, 3584 CT Utrecht, The Netherlands
[i] Howard Hughes Medical Institute, Chevy Chase, MD 20815, USA
[j] Koch Institute for Integrative Cancer Research, Massachusetts Institute of Technology, Cambridge, MA 02139, USA

ARTICLE INFO

Article history:
Received 11 February 2016
Returned to author for revisions
13 April 2016
Accepted 15 April 2016

Keywords:
HCV
Single-molecule FISH
Viral replication
Host–virus interactions

ABSTRACT

Hepatitis C virus (HCV) is a positive single-stranded RNA virus of enormous global health importance, with direct-acting antiviral therapies replacing an immunostimulatory interferon-based regimen. The dynamics of HCV positive and negative-strand viral RNAs (vRNAs) under antiviral perturbations have not been studied at the single-cell level, leaving a gap in our understanding of antiviral kinetics and host–virus interactions. Here, we demonstrate quantitative imaging of HCV genomes in multiple infection models, and multiplexing of positive and negative strand vRNAs and host antiviral RNAs. We capture the varying kinetics with which antiviral drugs with different mechanisms of action clear HCV infection, finding the NS5A inhibitor daclatasvir to induce a rapid decline in negative-strand viral RNAs. We also find that the induction of host antiviral genes upon interferon treatment is positively correlated with viral load in single cells. This study adds smFISH to the toolbox available for analyzing the treatment of RNA virus infections.

© 2016 Published by Elsevier Inc.

1. Introduction

Hepatitis C virus (HCV) chronically infects the liver hepatocytes of around 150 million people worldwide, and is a major cause of end-stage liver disease (Shepard et al., 2005). It is a single-stranded, positive sense RNA virus that uses its 9.6 kb genome as a template for both translation of the viral polyprotein and transcription of the negative strand RNA intermediate (Moradpour et al., 2007). Historically, treatment options for HCV have consisted of immunity-enhancing interferon treatment, which is associated with low cure rates and harsh side effects (Garber, 2011). Recently, highly potent direct-acting antivirals (DAAs) have been developed against multiple viral targets and which have led to near complete HCV cure rates in single and combination therapy (Afdhal et al., 2014; Kowdley et al., 2014). However, high costs and the demographics of infected patients have limited global access to these therapeutics, and the large population of infected but undiagnosed people means HCV will continue to be a public health concern (Paul et al., 2014; Holmberg et al., 2013) on which further study is warranted.

Much work has been done to elucidate HCV replication dynamics and its relationship with the host cell response (Paul et al., 2014; Marukian et al., 2011; Guidotti and Chisari, 2006; Yang et al., 2011; Li et al., 2015; Kazakov et al., 2015), especially its induction

* Corresponding author at: Institute for Medical Engineering and Science, Massachusetts Institute of Technology, Cambridge, MA 02139, USA.
E-mail address: sbhatia@mit.edu (S.N. Bhatia).
[1] These authors contributed equally to the work.
[2] Current address: Department of Epidemiology, University of North Carolina, Chapel Hill, NC 27599.
[3] Current address: Division of Gastroenterology and Hepatology, Weill Cornell Medical College, New York, NY 10021.

http://dx.doi.org/10.1016/j.virol.2016.04.020
0042-6822/© 2016 Published by Elsevier Inc.

of and evasion from hepatocyte innate immunity (Lemon, 2010; Li and Lemon, 2013). The regulatory mechanisms governing the levels of HCV viral RNA and proteins in individual infected cells are of particular interest, as HCV is generally non-cytopathic and infects a minority of hepatocytes in the liver (Li et al., 2015; Liang et al., 2009). To this end, temporal profiling of patient viral loads upon treatment have enabled the development of detailed quantitative models for viral replication and antiviral efficacy at the patient level (Dahari et al., 2005; Guedj et al., 2013, 2014; Neumann et al., 1998; Perelson and Guedj, 2015; Rong and Perelson, 2013), but these studies do not provide the resolution necessary to measure viral and host transcriptional dynamics in single cells, which would provide unique information about the mechanism of host cell responses to infection and to antiviral therapies. Single-cell analyses have been used recently to advance our understanding of biochemical variation (Eldar and Elowitz, 2010; Raj et al., 2010; Raj and van Oudenaarden, 2009) at both basal levels and under perturbations such as infection (Snijder et al., 2009; Snijder and Pelkmans, 2011), and single-molecule RNA imaging (smFISH) in particular has uncovered extensive inter-cell differences in mRNA expression that underlie phenotypic variation (Raj and van Oudenaarden, 2009, 2008; Raj et al., 2008; Golding et al., 2005; So et al., 2011; Gandhi et al., 2011).

Quantitative, single-molecule techniques have begun to advance viral RNA (vRNA) imaging as well, with some reports applying single-mRNA imaging to the study of single viral genomes in individual viral particles (Jouvenet et al., 2009; Chou et al., 2013, 2012), and more recently to the analysis of HCV vRNA colocalization with components of infected cells (Shulla and Randall, 2015). Here, we extend these studies by using simple, fluorescently labeled short oligos (Raj et al., 2008) to demonstrate sensitive, specific imaging of both HCV positive and negative strands and reporter viruses, compatible with multiple in vitro infection models and both standard and superresolution imaging. We detail the quantitative response of positive and negative strand vRNAs to multiple DAAs and interferon (IFN) treatment at the single-cell level for the first time, observing distinct kinetics of viral inhibition induced by antivirals with differing mechanisms of action. Finally, by observing the heterogeneous response of individual HCV-infected cells to IFN treatment, we utilize simultaneous quantitative imaging of host mRNAs and vRNA to observe that HCV infection induces, and persists in spite of, strong upregulation of IFN-stimulated gene expression. Overall, our results extend the toolbox of methods available for the analysis of RNA viral infection and treatment.

2. Materials and methods

2.1. Cell culture

Huh-7 (Nakabayashi et al., 1982), Huh-7.5 (Blight et al., 2002), and a clone of Huh-7.5 stably integrating the NS3–4A activity reporter (Jones et al., 2010) were all propagated in a DMEM with L-glutamine (Cellgro)-based medium containing 100 U/mL penicillin, 100 μg/mL streptomycin (Cellgro), and 10% FBS (GIBCO). Primary human fetal liver cells (HFLCs) were isolated and plated as described (Andrus et al., 2011). Cultures were maintained in Hepatocyte Defined Medium (HDM) (BD Biosciences) plus L-glutamine and antibiotics. Induced pluripotent stem cell (iPSC)-derived hepatocyte-like cells (iHLCs) were derived and cultured as described (Schwartz et al., 2012; Si-Tayeb et al., 2010). For smFISH experiments, cultures were grown on 12 mm, circular, No. 1 glass coverslips (VWR) in 24-well plates. For Huh-7.5s, attachment to coverslips was improved by coating with rat tail collagen I (BD Biosciences) at 50 μg/mL in water for 1 h at 37 °C and then rinsing prior to seeding. HFLC attachment was enhanced by first coating with collagen and subsequently with poly-L-lysine hydrobromide (Sigma) at 100 μg/mL for 45 min at room temperature and then rinsing prior to seeding. To put iHLCs on coverslips, they were treated with accutase (Millipore) for 15–20 min until they balled up. Gentle pipetting was performed to remove the cells, and they were then plated onto Matrigel-coated coverslips.

2.2. Hepatitis C virus infection, antiviral treatment, and interferon treatment

Hepatoma and iHLC infections were performed with a replication-competent *Gaussia* luciferase-expressing reporter virus based on the efficient Jc1 HCV construct (Jc1-Gluc) (Pietschmann et al., 2006); stocks of this reporter were obtained as described (Marukian et al., 2008). HFLC infections were performed either with this Jc1 reporter or with an adapted HCV called J6/JFH Clone 2 (Walters et al., 2009). Titration on naïve Huh-7.5s was used to determine 50% tissue culture infectious dose ($TCID_{50}$) of stocks of these strains of HCV. For infection experiments, we employed three standard models of HCV infection: the Huh-7.5 hepatoma cell line (as well as the associated Huh-7 cell line and the clone of Huh-7.5 stably expressing the NS3–4A activity reporter as described below) (Lindenbach et al., 2005), primary human fetal hepatocytes (Andrus et al., 2011), and induced pluripotent stem cell-derived hepatocyte-like cells (Schwartz et al., 2012). Stocks were diluted in the appropriate culture medium to make an inoculum with final titer typically in the 10^5-10^6 $TCID_{50}$/mL range (MOI ranging from ~0.2–2). Cultures to be infected were incubated in inoculum for varying durations depending on the experiment. Subsequently, medium was typically changed every 24–48 h unless otherwise noted, and cultures were washed with culture medium three times between medium changes. To demonstrate that smFISH imaging of HCV genomes is replication-dependent, the HCV non-structural protein 5B (NS5B) polymerase inhibitor 2′-C-methyladenosine (2′CMA), with $EC_{50}=27$ nM (Lindenbach et al., 2005), was used to supplement both the inoculum and subsequent fresh medium at a concentration of 80^*EC_{50} (final 0.1% DMSO) and compared to a DMSO-only control. For antiviral experiments, human interferon β (IFN-β) (Calbiochem, used at 100 U/mL for comparative antiviral experiments, and 10 U/mL for host response experiments), sofosbuvir (10 uM; $EC_{50}\sim20$ nM (Health AGDo, 2014)), daclatasvir (1 nM; $EC_{50}\sim20$ pM (Agency, 2014a)), and simeprevir (400 nM; $EC_{50}\sim10$ nM (Agency, 2014b)) were used to treat cells at the above concentrations (chosen as 10^*EC_{90} based) in a final concentration of 0.1% DMSO, at indicated time points either before or after infection as described.

2.3. Single-molecule RNA FISH (smFISH)

smFISH on culture samples is performed as described in detail (Raj et al., 2008). All protocols are also available online at http://www.singlemoleculefish.com. Briefly, culture samples on coverslips are fixed in 4% w/v paraformaldehyde (Electron Microscopy Sciences) in PBS for 10 min After washing with PBS, samples can be maintained in PBS for at least one week at 4 °C. Six hours prior to hybridization with probes, samples are permeabilized by placing in 70% EtOH in water at 4 °C. Coverslips are incubated in hybridization buffer containing a probe set targeting the RNA species of interest (BioSearch Technologies; http://www.singlemoleculefish.com; sequences in sets shown here are provided in Supplemental information which are probe sets of 48 probes targeting the *Gaussia*-luciferase-expressing HCV reporter described above; we have successfully quantified HCV with various probe sets (Supplementary information) each probe of which is coupled to desired fluorescent molecule (typically Alexa594 or Cy5).

Multiple probe sets coupled to spectrally distinct probe sets can be hybridized to sample simultaneous for multiplexed imaging. Finally, samples are washed, during which time fluorescent molecules targeting antigens of interest or immunofluorescence antibodies can be incorporated as described (Raj et al., 2008), and subsequently mounted for imaging. In this study, endoplasmic reticulum staining was performed using the ER-ID Green assay kit (Enzo Life Sciences), and HCV non-structural protein 5A (NS5A) immunostaining was performed using mouse anti-NS5A (9E10) and goat anti-mouse Alexa Fluor 594 (Invitrogen).

2.4. Microscopy and image analysis

Standard epifluorescence microscopy can ascertain smFISH spots as described (Raj et al., 2008). All images were taken with a Nikon Ti-E inverted fluorescence microscope equipped with a 100X oil-immersion objective and a Photometrics Pixis 1024 CCD camera using MetaMorph software (Molecular Devices, Downington, PA). Z-stacks were obtained as described (Raj et al., 2008); typically, 20–30 planes separated by 0.4 μm was sufficient to comprehensively cover the target cells. Images presented as slices from the Z-stack or maximum intensity projections as described. Images were analyzed to extract data we show using custom software written in MATLAB (MathWorks), which can identify spots on individual channels, assess co-localization, and quantify spots. Briefly, a Laplacian of Gaussian (LoG) filter is used to filter out slowly-varying background noise and spots outside of the size and shape range for fluorescent foci (e.g. autofluorescent cellular components), and spot counts are determined by thresholding the filtered image, where the threshold is determined empirically by minimizing the sensitivity of spot counts to changes in threshold. Quantification has an upper-bound for each cell that depends on cell volume (height and cross-section), subcellular distribution of target RNA, quality of imaging, and signal-to-noise ratio. At later time-points post infection (~48 h), the number of positive strands as visualized using an Alexa594 fluorophore probe set typically was deemed too large to be counted computationally without significant error in a small portion of the cells. For these cells, an estimate was obtained by integrating the fluorescence intensity in a sum projection of the Z-stack for the cell and subtracting the local background, and comparing this quantity with that of countable cells to extrapolate an estimate (Tan and van Oudenaarden, 2010). In order to obtain spot intensity distributions, we used custom-written MATLAB software to reduce the stacked images to two-dimensional images by maximum projection, and fitted the fluorescent spots to a 2D Gaussian as the model for the point spread function. Single transcript intensity was defined as the integrated intensity of the spot using the two-dimensional Gaussian mask algorithm. Structured illumination microscopy (SIM) images were performed using a DeltaVisionOMX 3D Structured Illumination Microscope (Applied Precision, Issaquah, USA). Solid state lasers (405, 488, 593 nm) provided wide-field illumination and multi-channel images were captured simultaneously using 3 Photometrics Cascade (Photometrics, Tucson, USA) back-illuminated EM-CCD cameras. All data capture used an Olympus UPlanSApo 100 × 1.4NA oil objective and standard excitation and emission filter sets. 3D-SIM images were sectioned using a 125 nm Z-step size. Raw 3-phase images were processed and reconstructed using softWoRx (Applied Precision) as previously described (Gustafsson et al., 2008). Confocal microscopy images were taken using a Zeiss Axiovert Microscope (Carl Zeiss, Oberkochen, Germany) and a Perkin Elmer Ultraview Spinning Disk Confocal. Solid state lasers provided wide-field illumination and multi-channel images were captured using Hammamatsu ORCA-ER CCD camera (Bridgewater, NJ). All data capture used a Zeiss ApoChromAT 100 × 1.4NA oil objective and standard excitation and emission filter sets. Raw images were processed and reconstructed using Volocity software (Perkin Elmer, Waltham, MA).

2.5. HCV non-structural protein 3-4A (NS3–4A) activity reporter

As previously described (Jones et al., 2010), we developed a real-time fluorescence reporter of HCV infection based on monitoring NS3–4A protease activity. A clone of Huh-7.5 stably expressing the RFP-NLS-IPS was used to determine the correlation between smFISH imaging of HCV genomes and NS3–4A protease activity.

2.6. Strand specific qPCR of HCV RNA

Non-infectious positive strand standards were constructed by digesting a plasmid containing J6/JFH1 "Clone 2" virus (Catanese et al., 2013) with *Sac*I (New England Biolabs) and religating the backbone. After *Xba*I (New England Biolabs) digestion, this DNA was used in a T7 transcription reaction to yield a 3516nt RNA standard with intact 5′ and 3′ ends. For minus strand standard synthesis, we employed an overlap PCR approach to flip the orientation of the positive strand standard while preserving the appropriate ends. Generated RNA stocks of both strands were equilibrated via nanodrop to a calculated concentration of 10^{10} copies/μl. Standard curves were generated by serially diluting the RNA standards in the presence of fixed 50 ng amounts of total RNA from uninfected Huh-7.5 cells. For qPCR of unknown samples, RNA was isolated using the RNeasy Plus Mini kit (Qiagen) from infected Huh-7.5 cells. Approximately 50 ng of total RNA was then used for PolyAdenylation using *E. coli* PolyA Polymerase (New England Biolabs) using 1 mM ATP, 3 U E-PAP and 7.5 U RNAsin Plus RNAse inhibitor (Promega, Madison, WS) in a 5 μl total reaction volume, and incubated for 10 min at 37 °C followed by 20 min at 65 °C to inactivate the enzyme. The resulting RNA underwent reverse transcription using Superscript III (Life Technologies): to the 5 μl of poly-A tailed RNA, 2.5 pmol of tagged RT primer (5′-GAATCGAGCACCAGTTACGCATGCCGAGGTCGACTTCC-TAGATTTTTTTTTTTTTTTTTTVN-3′) was added along with 0.5 μl of 10 mM dNTPs, and incubated at 65 °C for 5 min before placing on ice. To this mixture the RT mix was added per reaction consisting of 1x RT Buffer, 50 mM DTT, 2.5 U RNAsin Plus RNAse inhibitor and 100 U Superscript III, to a final RT reaction volume of 10 μl. Samples were incubated at 55 °C for 10 min, 60 °C for 50 min and 85 °C for 5 min and held at 4 °C. Inferred from input RNA amounts, approximately 2 ng of the resulting cDNA was used per subsequent qPCR reaction using 2x FastStart SYBRGreen qPCR mix (Roche) following the manufacturer's instructions and using 2.5 pmol primer for the tag sequence (GAATCGAGCACCAGTTACGCATG) and either the positive strand primer (CTGGTCTCTCTGCAGATCATGT) or the negative strand primer (CTGCGTGAAGACAGTAGTTCCTCA) also at 2.5 pmol. For convenience in some experiments, we adapted the miScript RT kit (Qiagen) that employs a polyA-tailing and RT step with the above RT primer in a single reaction, to produce the necessary input for subsequent qPCR using HCV specific primers and the tag primer. qPCR was carried out using iQ5 thermal cyclers (BioRad) using the following cycling parameters: 95 °C for 10 min, 40 cycles of [95 °C for 15 s, 58 °C for 15 s, 72 °C for 20 s collecting fluorescence], 95 °C for 2 min, 55 °C for 2 min followed by fluorescence measurement for each 0.5 °C interval increase to 95 °C for the generation of melt curves. Non-strand specific qPCR for HCV RNA was carried out using MultiCode-RTx technology (Eragen Biosciences) as described previously (Mulligan et al., 2009).

2.7. Statistical analysis

Error bars plotted as standard deviation (σ) or as standard error of the mean (SEM) as noted. Statistical analysis performed

as described – two-tailed *t* test, one-way ANOVA with Tukey's post-test, linear regression, and *F* test for determining positivity of slope performed using GraphPad Prism 5 (GraphPad Software). Pearson correlation coefficients obtained using MATLAB (The MathWorks).

3. Results

3.1. Specific and sensitive single-molecule imaging of genomic vRNA

We first tested our ability to perform mRNA smFISH (Raj et al., 2008) on HCV, by developing fluorophore-tagged, short

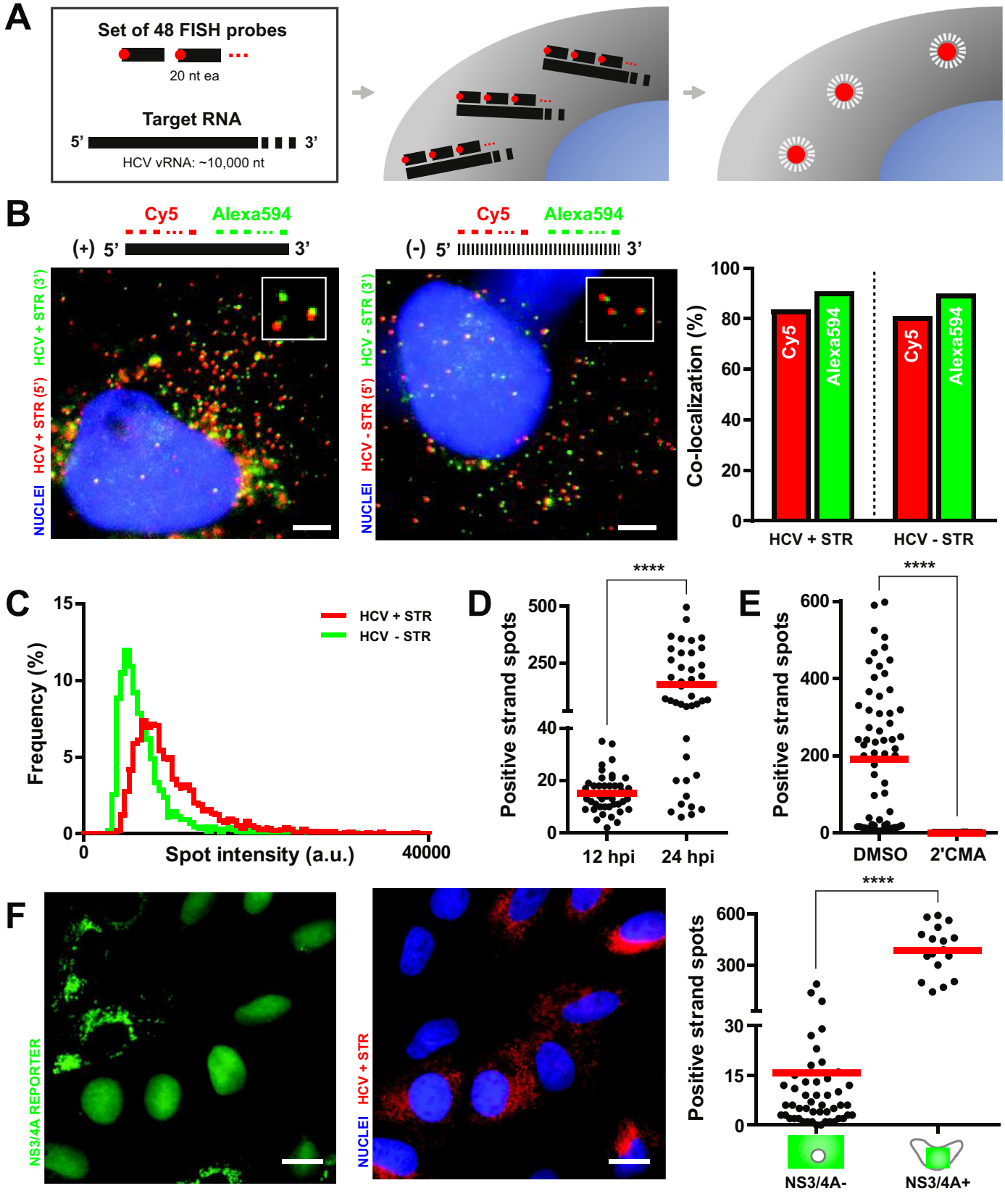

oligonucleotide probe sets for HCV RNA, which localize to produce diffraction-limited spots under standard epifluorescence microscopy after being delivered to fixed and permeabilized infected cells (Fig. 1A). To test the specificity of the method, we performed single-molecule vRNA imaging on HCV-infected Huh-7.5 cells (Blight et al., 2002; Lindenbach et al., 2005) using a Cy5 probe set targeting the 5′ half of the strand, and an Alexa594 probe set targeting the 3′ half, for both positive (+) and negative (−) strands. While smFISH performed on uninfected hepatoma cultures (Fig. S1A) or infected cultures without probes (Fig. S1B) both revealed no spots, infected cultures imaged simultaneously with both Cy5 and Alexa594 probe sets for either the positive or negative strand revealed diffraction-limited spots in both channels (Fig. 1B), with co-localization frequencies (> 80%) (Fig. 1B) similar to what has been observed for mRNAs (Raj et al., 2008). In order to assess whether vRNA spots represent single genomic strands, we employed a method previously reported for single molecule imaging whereby we integrated total spot fluorescence for many spots of both positive and negative-strand vRNA to determine whether the spot intensity was unimodal (Mutch et al., 2007), which would suggest spots are mostly single genomes. We found that the distribution of spot intensities was unimodal (Fig. 1C) and close to lognormal, suggesting that most spots represent single-molecule events, as previously seen with this technique (Vargas et al., 2005; Shalek et al., 2013), although the brightest data points within the distribution (at the far right of the *X* axis) may represent foci of viral transcription. Because HCV positive- and negative-stranded vRNAs can exist as duplexed dsRNA, which may not be accessible to our ssDNA probes, we examined the ability of smFISH to capture duplexed vRNAs by transfecting pre-complexed HCV dsRNA as a positive control and quickly fixing and imaging samples. We found that duplexed dsRNA is still detected as colocalized positive- and negative-strand vRNA, likely due to the denaturing hybridization conditions, suggesting that the smFISH protocol allows for probe binding to dsRNA (Fig. S1L).

Throughout the period we sampled, the number of HCV RNA spots increased with time post infection (Fig. 1D), and was greatly reduced in the presence of an antiviral compound, the HCV nonstructural protein 5B (NS5B) polymerase inhibitor 2′-C-methyladenosine (2′CMA) (Fig. 1E). We also compared the results obtained using vRNA smFISH to those using a highly sensitive, single-cell fluorescent reporter of HCV infection that discriminates infected from uninfected cells based on the protease activity of HCV nonstructural protein 3–4 A (NS3–4A) (Jones et al., 2010). In this assay, in the absence of NS3–4A activity (reporter negative), fluorescence is localized to the cytosol, whereas nuclear fluorescence is induced in infected cells that exhibit active NS3–4A (reporter positive), which cleaves the reporter to expose a nuclear localization signal, resulting in nuclear transport of the fluorescent tag. By combining these two methods, we observed significantly more smFISH spots present in reporter positive than reporter negative cells (Fig. 1F), providing an independent single-cell measure of infection to correlate with our vRNA imaging technique. Amongst the reporter negative cells, a range of smFISH spot counts were detected, suggesting that vRNA smFISH is even more sensitive than an enzymatic viral protein-driven reporter, and thus may detect infection at a lower viral load.

Since smFISH maintains spatial information and is compatible with most fluorescent imaging modalities and co-stains, we next tested whether we could perform smFISH of HCV using super-resolution three-dimensional structured illumination microscopy (3D-SIM) (Schermelleh et al., 2008). We observed co-localization of HCV positive strands jointly with the endoplasmic reticulum (ER), with which viral replication complexes associate (Fig. S1C) (Gosert et al., 2003; El-Hage and Luo, 2003), and also with HCV nonstructural protein 5A (NS5A) (Fig. S1D). We also sought to extend the utility of our method by testing it using authentic host cells, given that HCV host–virus interactions are more relevant when studied in non-transformed cell lines. To this end, we attempted smFISH using two primary hepatocyte models of HCV infection – induced pluripotent stem cell (iPS)-derived hepatocyte-like cells (iHLCs) (Schwartz et al., 2012) and primary human fetal liver cells (HFLCs) (Andrus et al., 2011). Infected iHLCs (Fig. S1E) and HFLCs (Fig. S1G), but neither uninfected iHLCs (Fig. S1F) nor uninfected HFLCs (Fig. S1H) demonstrate positive strand vRNA smFISH spots, with fewer strands detected in the presence of 2′CMA (Fig. S1I). While only 40% of HFLCs were reporter positive in replicate samples, at least one viral genome was detected in 93% of HFLCs, suggesting improved sensitivity of the smFISH method (Fig. S1J). Because virus-infected cells can undergo coinfection or superinfection, we wanted to determine if our smFISH method could facilitate orthogonal imaging of multiple viral variants. To do this, we synthesized a fluorescently-tagged set of probes complementary to the genomic sequence of a tagRFP reporter inserted into a reporter HCV genome, and demonstrated specific targeting of this exogenous viral sequence (Fig. S1K) as well as targeting of an exogenous luciferase viral reporter (data not shown).

3.2. Single-cell, multiplexed quantification of viral positive and negative strands enable studies of the viral life cycle

Having established smFISH as a specific and sensitive method to visualize HCV infection in a range of hepatic cells, we next applied the technique to study viral replication dynamics by simultaneously enumerating positive and negative strand spots within individual cells. Huh-7.5 cells were infected with HCV and fixed at various hours post infection (hpi) (Fig. 2A). Multiplexed imaging was performed using two spectrally distinct probe sets, each targeting a different vRNA strand (Fig. 2A). At each time point, the resulting images (Fig. 2B) yielded a single-cell joint distribution of positive and negative strand spot counts that evolved over time. We averaged positive and negative strand data over many cells (Fig. 2C) to measure how average negative-to-positive strand ratios (NPSR) vary over time (Fig. 2C, *Inset*). We also

Fig. 1. Specific and sensitive imaging of individual molecules of genomic viral RNA (vRNA). (A) Schematic illustration of single-molecule RNA FISH (smFISH) method (Raj et al., 2008). A set of 48 DNA FISH probes (20 nucleotides/probe) that are each end-labeled with one fluorophore (red) and that are complementary to non-overlapping portions of the target RNA (*Left*) are introduced to fixed and permeabilized cells. Hybridization of probes to the target RNA (Center) produces sufficient local fluorescence for the RNA molecule to be visualized as a diffraction-limited spot using standard epifluorescence microscopy (*Right*); spots are detected only once a minimum number of probes (typically ~20 (Raj et al., 2008)) bind the target. (B) Co-localization of diffraction-limited spots in infected Huh-7.5 hepatoma cultures (16 h post infection) was detected by simultaneously introducing two spectrally-distinct probe sets (coupled to Cy5 and Alexa594 respectively) targeting different portions of the same genomic vRNA strand. Typical images of positive (*Left*, Z-stack projection, scale bar ≈ 5.0 μm; *Inset*, ~2x zoom) and negative (Center, Z-stack projection, scale bar ≈ 4.0 μm; *Inset*, ~2x zoom) strand spots shown. Percentage of Cy5 and Alexa594 spots that co-localize with the other channel are shown for both strands (*Right*). (C) The integration of the range of spot intensities observed are presented as a histogram of the distribution of intensities for spots measured 24 h post infection (hpi) for both strands. (D) Number of positive strand spots in individual cells at 12 and 24 hpi (red line = mean). Difference was statistically significant: $^{****}p < 0.0001$ (two-tailed *t* test). (E) Number of positive strand spots in individual cells in DMSO or the HCV NS5B polymerase inhibitor 2′CMA at 24 hpi (red line = mean). Difference was statistically significant: $^{****}p < 0.0001$ (two-tailed *t* test). (F) NS3–4A activity reporter (Jones et al., 2010) deems cells infected based on nuclear fluorescence and uninfected based on cytosolic fluorescence. The Huh-7.5 Clone 8 line which carries this reporter stably was used to compare NS3–4A imaging with smFISH. Sample images from the same field of view for both NS3–4A reporter (*Left*, scale bar ≈ 18.5 μm) and smFISH (Center, ≈ 18.5 μm) are shown. Number of positive strand spots in reporter negative or reporter positive cells 24 hpi are provided (red line = mean) (*Right*). $^{****}p < 0.0001$ (two-tailed *t* test).

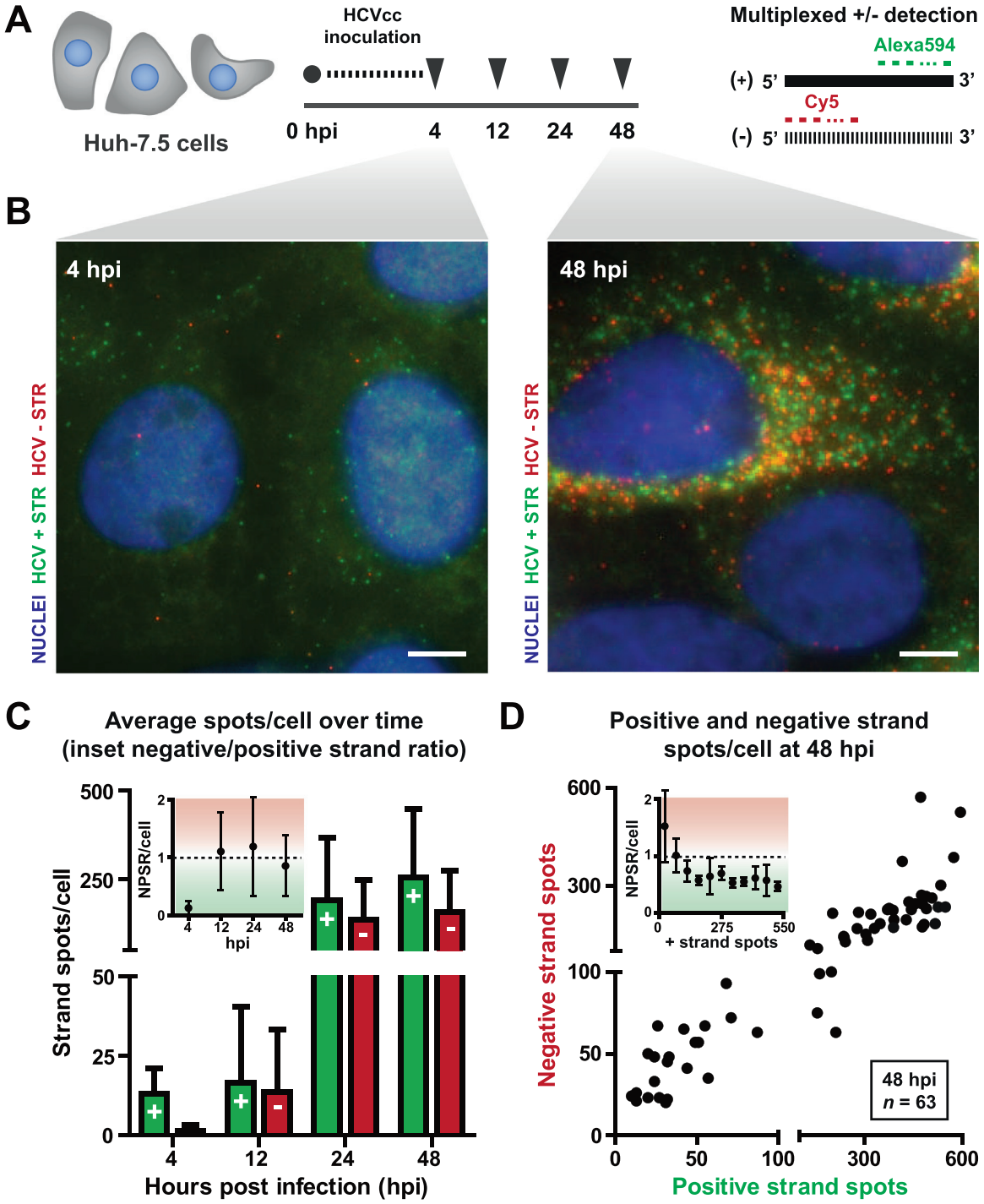

Fig. 2. Multiplexed quantification of positive and negative viral strands in individual cells. (A) Schematic illustration of experiment. Huh-7.5 hepatoma cells were inoculated with HCV for 4 h, and then fixed (triangles) for smFISH at various times thereafter (*Left*). Multiplexed imaging was performed by simultaneously employing an Alexa594 probe set for the positive strand and a Cy5 probe set for the negative strand (*Right*). (B) Sample images at 4 (*Left*, Z-stack projection, scale bar $\approx 7.0\,\mu m$) and 48 hpi (*Right*, Z-stack projection, scale bar $\approx 6.0\,\mu m$). (C) The average number of positive and negative strand spots observed per cell are plotted for each timepoint (4 hpi: $n=70$ cells; 12 hpi: $n=44$ cells; 24 hpi: $n=67$ cells; 48 hpi: $n=63$ cells). Data plotted as mean $\pm$ standard deviation The average single cell negative: positive strand ratio (NPSR) at each timepoint are plotted as mean $\pm$ standard deviation (*Inset*). (D) The absolute number of positive and negative strand spots per individual cell at 48 hpi are presented as a scatter plot ($n=63$) (Pearson correlation coefficient $\rho=0.86$). Axes are split into two linear segments each: 0–100, 100–600. After binning cells by intervals of 50 positive strand spots, the average single-cell NPSR was calculated for each bin, and is plotted as mean $\pm$ standard deviation (*Inset*).

present single-cell data for viral RNAs and NPSR dependence on infection load at 48 hpi (Fig. 2D). While significant inter-cell heterogeneity was detected, positive and negative strand vRNAs were correlated at the single-cell level. Because the Jc1-Gluc virus is replication-competent, the low-strand spot cells at late timepoints may represent cells newly infected by virus produced in culture. Infected cells also cluster bimodally into subpopulations bearing low or high strand counts (Fig. S2).

In order to cross-validate our vRNA measurements with an independent assay, we developed a new PCR assay that improves our capacity to discriminate between positive and negative strand vRNAs, since the application of previously published methods

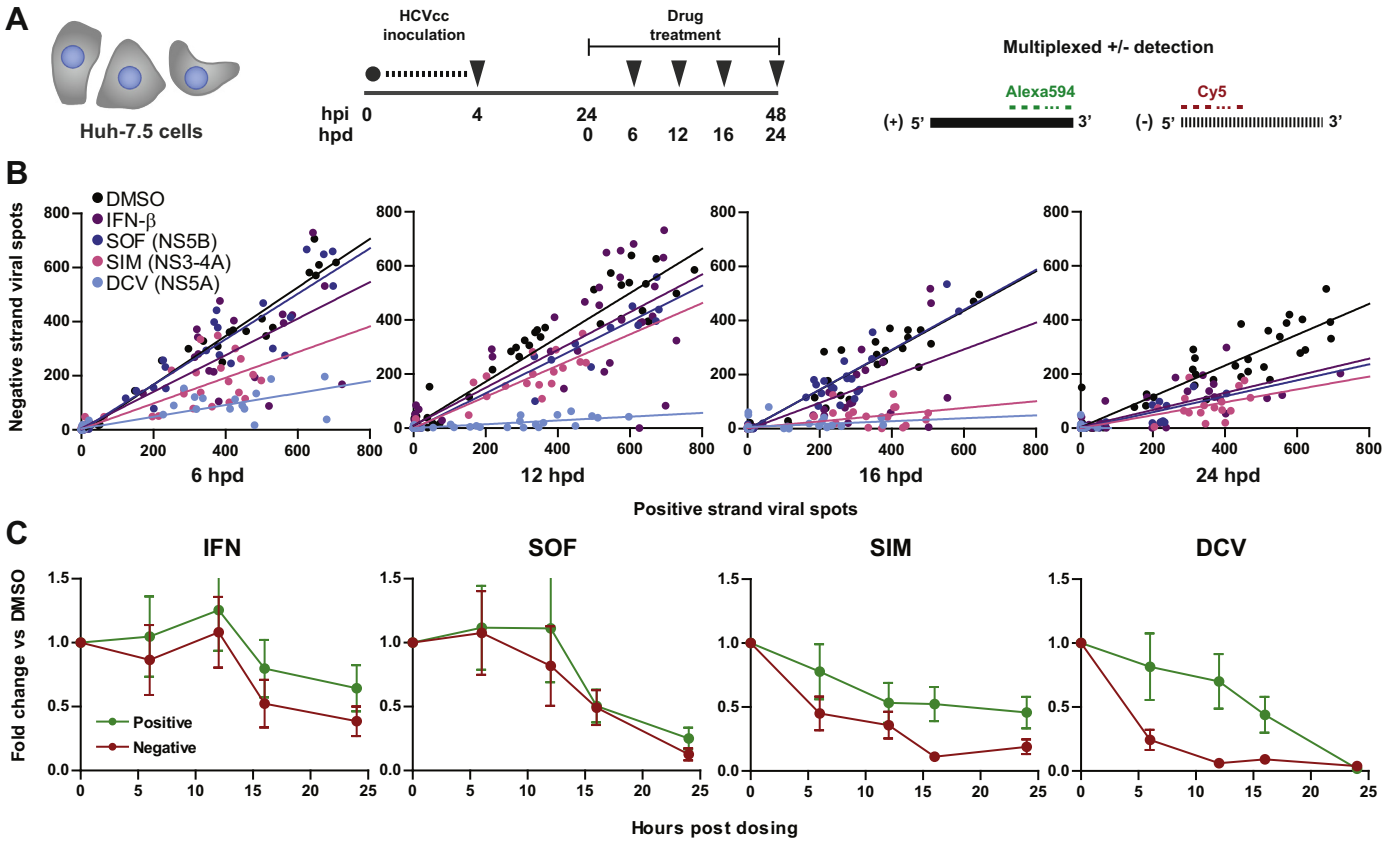

Fig. 3. Kinetics of vRNA expression during antiviral drug treatment. (A) Schematic illustration of experiment. Huh-7.5 hepatoma cells were inoculated with HCV for 4 h, and then drug treatment was started at 24 hpi. Cells were fixed for staining (triangles) at various times post infection (hours post dosing (hpd)=hpi – 24) (*Left*). Multiplexed imaging was performed by simultaneously employing an Alexa594 probe set for the positive strand and a Cy5 probe set for the negative strand (*Right*). (B) Scatter plots of positive and negative strand spot counts per cell, over time (6, 12, 16, and 24 hpd) during treatment with each antiviral compound (IFN-beta, SOF, SIM, DCV), or DMSO control. Linear best-fit lines for each condition are included to aid in visualization of HCV viral strand skew in response to each antiviral. (C) The average number of positive or negative strand spots per cell were calculated at each timepoint, and the resulting values for each antiviral treatment were normalized relative to the number of positive and negative strands in DMSO controls (n=35–85 per data point), to give a population-wide perspective of the impact of drug treatment on each sense of viral RNA. Data are plotted as mean ± SEM.

yield NPSR values for HCV that range widely from 1:10 to 1:1000, and these readings have been confounded by both interference from the opposite strand, and detection of incomplete vRNAs (McGuinness et al., 1994; Revie and Salahuddin, 2011; Agnello et al., 1998; Komurian-Pradel et al., 2004; Lanford et al., 1995; Lohmann et al., 1999). In this updated assay, total RNA is poly-A tailed, after which a tag oligo-dT anchored primer is used to reverse transcribe from the nascent tail (Fig. S3A); the resulting complementary DNA (cDNA) is then used for qPCR, employing a primer for the tag sequence and an HCV-specific primer for the 3′ end of the target vRNA. This assay offers two main updates relative to previously employed tagged assays (Agnello et al., 1998; Komurian-Pradel et al., 2004; Lanford et al., 1995), in that strand specificity is introduced at the PCR stage, and amplicons are generated that straddle the 3′ ends of completed positive and negative strand products of the viral polymerase. Using standards for both strands individually, we confirmed that the assay is sensitive over 8 logs for either strand (Fig. S3B). In addition, we used mixtures of positive and negative strand standards to determine that both strands could be detected unambiguously within a large range; single negative strands could be reliably detected in the presence of 10^3 positive strands, while positive strands could be detected in up to 100-fold excess of negative strands (Fig. S3C). Using PAqPCR to measure vRNA side-by-side with smFISH on replicate samples, we found that both assays yielded a similar fold change in positive or negative strand vRNA between two time points post infection (Fig. S3D and E), suggesting that smFISH can be considered quantitative when used to enumerate both positive and negative strands.

3.3. *smFISH elucidates the single-cell response of infected cells to antiviral drugs*

After validating the strand-specific and quantitative data gleaned via smFISH of vRNA, we sought to determine whether this same technique could be used to detect differing antiviral signatures. To this end, we investigated the impacts of four compounds that function via distinct mechanisms of action: IFNβ, a virus-induced host signaling protein that induces interferon-stimulated genes (ISGs) with antiviral activity; and three direct-acting *anti*virals: sofosbuvir (SOF), a nucleotide analog and inhibitor of the HCV polymerase NS5B; daclatasvir (DCV), an inhibitor of the multifunctional HCV protein NS5A; and simeprevir (SIM), an inhibitor of the HCV protease NS3–4A. We infected Huh-7.5 cells with HCV for 4 h, and at 24 hpi, cultures were treated with each of the compounds and fixed at 6, 12, 16, and 24 h post dosing (hpd) for smFISH analysis (Fig. 3A). The single-cell bivariate data for positive and negative strands (Fig. 3B) reveal varied response characteristics between drug treatments, and in particular the cellular response to IFN treatment appears more heterogeneous in its strand skew than the response to DAA treatment.

To enable the drawing of more specific inferences regarding drug effects and mechanisms, we aggregated the data and normalized the responses relative to the DMSO control (Fig. 3C) to

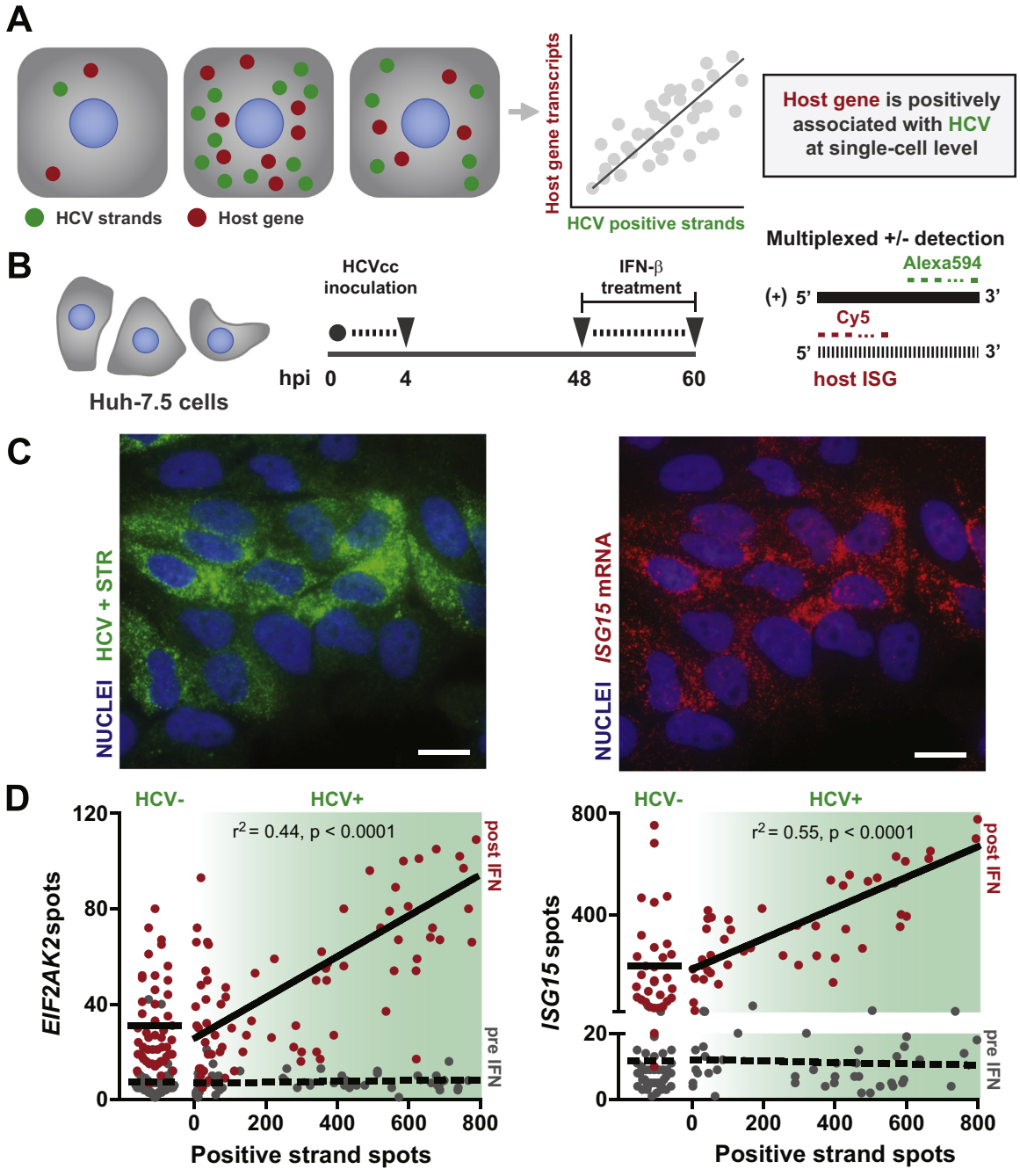

Fig. 4. Multiplexed quantification of viral positive strands and host mRNA transcripts in individual cells. (A) Schematic illustration of concept. The presence of correlated infection and host gene expression at the single-cell level (*Top*) can be identified using multiplexed smFISH to plot data that yields a single-cell joint distribution for a vRNA and host gene of interest (*Bottom Left*). By analyzing the relationship between vRNA levels and host gene levels on a per-cell basis, hypotheses about host gene regulation of vRNAs, or vice versa, can be generated and tested. For example, if host gene distribution is unperturbed upon infection, but vRNA levels are higher in cells with more host gene spots, pathways mediated by the assayed host gene may boost viral replication (*Bottom Right*). (B) Schematic illustrating the experiment, designed to ascertain the presence or absence of a relationship between HCV infection and interferon-stimulated gene (ISG) expression by dosing with the Type I interferon (IFN), IFN-β. Multiplexed smFISH for HCV positive strand spots and either *EIF2AK2* or *ISG15* spots is performed on infected (48 hpi) or uninfected cells before or after dosing with 10 U/mL IFN-β for 12 h. (C) Multiplexed images of HCV positive strand spots (*Left*), and *ISG15* mRNA (*Right*) in the same field of view (scale bar ≈ 17.0 μm), 12 h post dosing of IFN-β. (D) Scatter data plots the joint distribution for the number of two different ISG mRNA transcript spots (*EIF2AK2, Left* and *ISG15*, *Right*) versus positive HCV strand spots in individual, infected cells. In each plot, controls are presented on the left side of the *X* axis (HCV-), such that each point represents the number of ISG mRNA spots in individual, uninfected cells. The left-to-right green gradient tracks the increasing viral load within infected cells, based on the number of HCV positive strand spots. Gray dots represent the spot counts in cells prior to IFN treatment (dashed mean and best-fit lines included), whereas red dots are data points that result post-IFN treatment (solid mean and best-fit line). Prior to IFN stimulation, infected cells showed no positive correlation between ISG mRNA expression and HCV positive strand spots for either ISG (*EIF2AK2*, $p > 0.05$; *ISG15*, $p > 0.05$), as determined by an *F* test on linear regression parameters. However, a strong positive correlation between both ISG mRNA and HCV positive strand spots was observed (*EIF2AK2*, $p < 0.0001$; *ISG15*, $p < 0.0001$) after IFN treatment, as determined by an *F* test on linear regression parameters.

yield a strand-specific viral decay time course for each treatment. All 4 treatments produced a noticeable impact on viral RNAs by 24 hpd; however, the kinetics of viral decay varied significantly between groups. Response to IFN was delayed relative to the DAA treatments, and among the DAAs, patterns of strand decay varied greatly, with concordant decay between positive and negative

strands upon SOF treatment, but rapid, selective negative strand depletion upon DCV treatment.

3.4. Single-cell, multiplexed imaging of viral strands and host genes track host–virus interactions

Since interferon-mediated clearance depends on host cell responses, and our single-cell observations revealed cell-to-cell variability in viral clearance upon interferon treatment, we sought to look more directly at this phenomenon by harnessing the capacity of smFISH to simultaneously measure viral RNA and host mRNA in individual host cells (Fig. 4A). IFN stimulation initiates a JAK/STAT signaling cascade that culminates in the induction of antiviral interferon-stimulated genes (ISGs) (Schoggins et al., 2011; Theofilopoulos et al., 2005; Sadler and Williams, 2008). We developed smFISH probe sets that target mRNA transcripts for two prototypical ISGs with anti-HCV activity (Metz et al., 2013): *EIF2AK2/PKR*, which phosphorylates EIF2α to reduce host translation and inhibit HCV (Garaigorta and Chisari, 2009; Chang et al., 2006), and *ISG15*, a multifunctional protein which "ISGylates" proteins for targeted degradation (Chen et al., 2011). As a positive control, uninfected Huh-7.5 cells treated with IFN-β for 6, 12, or 24 h were fixed and assayed by smFISH. As expected, the baseline *EIF2AK2* and *ISG15* transcript levels were visualized as diffraction-limited spots that rapidly increased in number upon administration of IFN-β (Figs. S4A and B, and 4D), and reached a stable plateau for at least 6–24 h (Fig. S4B). Notably, despite uniform administration of IFN-β, ISG expression varied significantly between individual cells in the treated population. In order to determine whether the induction of ISG expression upon IFN treatment correlated with vRNA levels, infected Huh-7.5 cells were fixed for multiplexed imaging of HCV vRNA with either *ISG15* or *EIF2AK2,* before or after a 12 h exposure to IFN-β (Fig. 4B). In the absence of IFN-β, hepatoma cells did not upregulate ISG mRNAs upon infection (Fig. 4D), and no correlation was observed between ISG mRNA and HCV vRNA levels (Fig. 4D, gray). This observation is consistent with reports of a defective RIG-I sensing of HCV vRNA in Huh-7.5s (Sumpter et al., 2005). However, after treatment with exogenous IFN-β, while HCV strand counts were not significantly reduced (Fig. S4C), the levels of both ISG mRNAs positively correlated with HCV infection load (Figs. 4C and D, red, S4D), and ISG levels observed in poorly infected cells were similar to those detected in uninfected controls (Fig. 4D, red). To better visualize this trend, we binned individual cells into groups with "low" and "high" levels of infection (Fig. S4E), and observed that only highly infected cells harbor significantly more ISG mRNAs than uninfected controls (Fig. S4F). These data suggest that although HCV can subvert hepatocyte innate immunity in multiple ways (Horner and Gale, 2009; Heim et al., 1999; Lin et al., 2006), viral products stimulate, rather than repress, ISG transcription upon IFN treatment.

4. Discussion

In this study, we demonstrated sensitive, specific, and quantitative imaging of HCV and other viral RNAs (tagRFP reporter sequence, Fig. S1K; DENV-2, data not shown). We demonstrated multiplexing of positive and negative vRNA strands, vRNA with host ER and viral proteins, and vRNA with host cell mRNAs (Figs. S1C and D; 2–4). Furthermore, we highlighted the applicability of this approach to primary cell infection models (Fig. S1E-H) that more closely recapitulate physiological infection of quiescent cells with normal host gene expression and intact innate immune signaling (Sumpter et al., 2005; Durantel and Zoulim, 2007; Mee et al., 2008). While a previous smFISH analysis of HCV (Shulla and Randall, 2015) focused on colocalization of vRNAs with ribosomes and viral proteins, here we extend the application of vRNA smFISH to the study of host-pathogen interactions downstream of IFN signaling, and viral clearance upon antiviral treatment.

Using our specific and quantitative approach, verified using our novel PCR-based bulk assay (Fig. S2), we demonstrate that while the general understanding has been that positive strands greatly outnumber negative strands in ssRNA(+) viruses (Ahlquist et al., 2003; Buck, 1996), we find that this ratio varies significantly with time. We observed that the mean single-cell NPSR starts low at 4 hpi, consistent with early virion unpacking and minimal replication, and in Huh-7.5 cells this ratio increases, followed by possible tapering thereafter (Fig. 2C, *Inset*). The data at 48 hpi shows that NPSR appears negatively correlated with positive strand spots at the single-cell level until approximately ~200 positive-strand spots, with a more stable distribution above this number (Fig. 2D, *Inset*), mirroring the population-scale NPSR trends. One hypothesis is that negative strand production may peak at lower single-cell viral loads in order to produce the templates that enable subsequent rapid replication of positive strands, followed by a transition from transcription-dominant to translation-dominant production of new viral species from positive strand vRNAs. Since the Jc1-Gluc virus produced in culture can reinfect Huh-7.5 cells, it is possible that cells with low positive-strand spot counts at late timepoints like 48 hpi represent secondary infection events from culture-derived virus. In this case, the more stable NPSR at higher positive-strand counts could indicate the greater stability of this ratio at longer times post-infection in a given cell.

The high-resolution strand-specific data enabled by smFISH also provides interesting information relating to HCV antivirals and their mechanisms of action (Fig. 3B and C) (Guedj et al., 2014, 2013; Rong and Perelson, 2013). The delayed, robust response to IFN, for example, may be due to the time required for cellular antiviral proteins to be induced, transcribed, and translated upon IFN treatment. Furthermore, while treatment with the polymerase inhibitor, SOF, led to a balanced decay of both positive and negative strands, by blocking template transcription from both positive and negative strand vRNAs, the NS5A inhibitor DCV caused a skewed depletion of negative strand vRNAs with a shorter-than-expected half-life of 3 h (Guedj et al., 2013, 2013; Quinkert et al., 2005; Binder et al., 2013). Indeed, across all treatments, very few cells exhibited a strand skew that favored negative strand vRNAs. This finding may suggest the negative strand is intrinsically less stable, a hypothesis that is consistent with previous reports suggesting the negative strand is less stable due to fewer interactions with miR-122 (Li et al., 2015; Shimakami et al., 2012) or other factors. However, since both NS5A inhibitors and HCV protease inhibitors have been shown to inhibit viral assembly and/or release (Guedj et al., 2013; McGivern et al., 2014), the measured positive strand decline with these drugs (DCV and SIM) may be slowed somewhat by retention of otherwise-exported positive strand vRNAs.

The single cell data collected will likely be compatible with integration into existing computational frameworks that model HCV replication and treatment (Dahari et al., 2005; Guedj et al., 2014; Binder et al., 2013; Dahari et al., 2007, 2009), where the rates of strand-specific vRNA decay can shed light on which components of the viral life cycle are affected by therapeutics. For example, we are intrigued by the rapid effects of DCV on HCV negative strand vRNA, which had not been identified in a previous non-strand specific analysis of DCV temporal effects (Guedj et al., 2013). Considering this result, and based on a sensitivity analysis performed in a recent computational HCV model (Binder et al., 2013), it would be interesting to explore whether inhibitory effects of DCV on NS5A-associated replication complexes serve as important drivers of rapid negative strand decline, as NS5A relocalization from RCs (Lee et al.,

2011) may sensitize negative strands to rapid degradation. While the DAAs employed here were selected based on their known viral targets, future smFISH-mediated studies of post-treatment viral kinetics may provide insights into antiviral mechanism of action by matching strand-specific vRNA kinetic profiles to drugs with known mechanism, and offer a framework for the comparison of novel drugs or drug combinations.

Compared to the DAAs, IFN produces a more variable response to HCV across a population of individual cells, which we aimed to dissect in more detail by simultaneously measuring vRNAs and host antiviral mRNAs induced by IFN treatment. HCV possesses numerous ways to evade hepatocyte innate immunity, both upstream and downstream of cell-intrinsic Type I IFN production, such as the cleavage of MAVS and TRIF by the NS3–4A protease, induction of SOCS3 to block JAK/STAT signaling by HCV Core, and induction of PP2A and PKR which also block ISG transcription and translation, respectively (Horner and Gale, 2009; Gale and Foy, 2005; Wong and Chen, 2014). Because HCV can dampen the IFN cascade at numerous stages, which may confound interpretation of its inhibitory effect, we used smFISH to specifically look at whether HCV prevented accumulation of ISG transcripts soon after IFN treatment. In stark contrast, we found that after treatment with exogenous IFN-β, ISG mRNAs positively correlated with HCV infection load (Figs. 4C and D, and S4D). While the innate immune axis in Huh-7.5 cells is known to be compromised in RIG-I signaling (Sumpter et al., 2005), our analysis takes place downstream of IFN-β signaling and corroborates recent results in treatment-naïve, HCV-infected patient liver tissue, where hepatocytes positive for HCV vRNA by bDNA-FISH also contained significantly more IFI27 mRNA (Wieland et al., 2014). It is possible that within our experimental timeframe, the effect of HCV upregulation of SOCS3 and other inhibitors of JAK/STAT signaling is not yet evident, but also highlights the fact that high ISG transcript levels do not correlate with clearing infection, even in patients treated with IFN (Sarasin-Filipowicz et al., 2008). Indeed, the post-transcriptional blockage of ISG effectors by HCV, for example, via induction of PKR (Garaigorta and Chisari, 2009), may inhibit antiviral responses even in the presence of upregulated ISG transcription.

In summary, this study provides evidence for the numerous ways in which quantitative vRNA imaging can boost our understanding of HCV, and RNA viruses more generally, by providing single-cell traces of responses to antiviral drugs, and allowing for single-cell correlative measures of host and viral responses. Our inexpensive smFISH technique for quantitating vRNA functions at an efficiency that is on par with a proprietary branched DNA amplification method recently used to detect single HCV vRNAs (Shulla and Randall, 2015), and can be integrated with rapid-staining techniques for increased throughput (Shaffer et al., 2013). This toolbox can be extended by offering simultaneous single-cell protein and RNA-level imaging when combined with fluorescent reporter viruses and integration with flow-based quantification (Robertson et al., 2010; Bushkin et al., 2015), or by simultaneous monitoring of two viral mutants with appropriate reporter sequences to study questions of drug resistance and superinfection (Tscherne et al., 2007).

Acknowledgments

We thank Dr. Heather Fleming for significant assistance in manuscript preparation, and Dr. Andrea Branch for valuable advice on experimental design. Further, we thank Dr. Alice Chen, Dr. Tal Danino, and Dr. Sabine Hauert for insightful discussions, and Eliza Vasile at the Koch Institute Microscopy center for help with SIM microscopy. This work was performed with the generous support of the National Institutes of Health (NIH) Grants from NCI (1 R01 CA057973), NIAID (1 R01 AI099284), the Office of the Director and the NIDDK NIH Roadmap for Medical Research (1 R01 DK085713), The Greenberg Medical Research Institute, the NIH/NCI Physical Sciences Oncology Center at MIT (U54 CA143874), a NIH Pioneer award (1DP1 OD003936), The Starr Foundation, the Fannie and John Hertz Foundation, and the NSF GRFP (V. R.). S. N. B is a Howard Hughes Medical Institute Investigator. The authors declare no conflicts of interest.

Appendix A. Supplementary material

Supplementary data associated with this article can be found in the online version at http://dx.doi.org/10.1016/j.virol.2016.04.020.

References

Afdhal, N., Reddy, K.R., Nelson, D.R., Lawitz, E., Gordon, S.C., Schiff, E., Nahass, R., Ghalib, R., Gitlin, N., Herring, R., Lalezari, J., Younes, Z.H., Pockros, P.J., Di Bisceglie, A.M., Arora, S., Subramanian, G.M., Zhu, Y., Dvory-Sobol, H., Yang, J.C., Pang, P.S., Symonds, W.T., McHutchison, J.G., Muir, A.J., Sulkowski, M., Kwo, P., 2014. Ledipasvir and Sofosbuvir for previously treated HCV genotype 1 infection. N. Engl. J. Med. 370, 1483–1493.

Agency EM. 2014a. Daklinza, INN-daclatasvir.

Agnello, V., Ábel, G., Knight, G.B., Muchmore, E., 1998. Detection of widespread hepatocyte infection in chronic hepatitis C. Hepatology 28, 573–584.

Ahlquist, P., Noueiry, A.O., Lee, W.-M., Kushner, D.B., Dye, B.T., 2003. Host factors in positive-strand RNA virus genome replication. J. Virol. 77, 8181–8186.

Andrus, L., Marukian, S., Jones, C.T., Catanese, M.T., Sheahan, T.P., Schoggins, J.W., Barry, W.T., Dustin, L.B., Trehan, K., Ploss, A., Bhatia, S.N., Rice, C.M., 2011. Expression of paramyxovirus V proteins promotes replication and spread of hepatitis C virus in cultures of primary human fetal liver cells. Hepatology 54, 1901–1912.

Binder, M., Sulaimanov, N., Clausznitzer, D., Schulze, M., Hüber, C.M., Lenz, S.M., Schlöder, J.P., Trippler, M., Bartenschlager, R., Lohmann, V., Kaderali, L., 2013. Replication vesicles are load- and choke-points in the hepatitis C virus lifecycle. Plos Pathog. 9, e1003561.

Blight, K.J., McKeating, J.A., Rice, C.M., 2002. Highly permissive cell lines for subgenomic and genomic hepatitis C virus RNA replication. J. Virol. 76, 13001–13014.

Buck, K.W., 1996. Comparison of The Replication of Positive-Stranded Rna Viruses of Plants and Animals. In: Karl Maramorosch, F.A.M., Aaron, J.S. (Eds.), Adv Virus Res Volume 47. Academic Press, Cambridge, MA, USA, pp. 159–251.

Bushkin, Y., Radford, F., Pine, R., Lardizabal, A., Mangura, B.T., Gennaro, M.L., Tyagi, S., 2015. Profiling T cell activation using single-molecule fluorescence in situ hybridization and flow cytometry. J. Immunol. 194, 836–841.

Catanese, M.T., Loureiro, J., Jones, C.T., Dorner, M., von Hahn, T., Rice, C.M., 2013. Different requirements for scavenger receptor class B type I in hepatitis C virus cell-free versus cell-to-cell transmission. J. Virol. 87, 8282–8293.

Chang, K.-S., Cai, Z., Zhang, C., Sen, G.C., Williams, B.R.G., Luo, G., 2006. Replication of hepatitis C virus (HCV) RNA in mouse embryonic fibroblasts: protein kinase R (PKR)-dependent and PKR-independent mechanisms for controlling HCV RNA replication and mediating interferon activities. J. Virol. 80, 7364–7374.

Chen, L., Li, S., McGilvray, I., 2011. The ISG15/USP18 ubiquitin-like pathway (ISGylation system) in hepatitis C virus infection and resistance to interferon therapy. Int. J. Biochem. Cell Biol. 43, 1427–1431.

Chou, Y.-y., Vafabakhsh, R., Doğanay, S., Gao, Q., Ha, T., Palese, P., 2012. One influenza virus particle packages eight unique viral RNAs as shown by FISH analysis. Proc. Natl. Acad. Sci. U.S.A. 109, 9101–9106.

Chou, Y.-y., Heaton, N.S., Gao, Q., Palese, P., Singer, R., Lionnet, T., 2013. Colocalization of different influenza viral RNA segments in the cytoplasm before viral budding as shown by single-molecule sensitivity FISH analysis. Plos Pathog. 9, e1003358.

Dahari, H., Ribeiro, R.M., Rice, C.M., Perelson, A.S., 2007. Mathematical modeling of subgenomic hepatitis C virus replication in Huh-7 cells. J. Virol. 81, 750–760.

Dahari, H., Sainz, B., Perelson, A.S., Uprichard, S.L., 2009. Modeling subgenomic hepatitis C virus RNA kinetics during treatment with alpha interferon. J. Virol. 83, 6383–6390.

Dahari, H., Major, M., Zhang, X., Mihalik, K., Rice, C.M., Perelson, A.S., Feinstone, S. M., Neumann, A.U., 2005. Mathematical modeling of primary hepatitis C infection: noncytolytic clearance and early blockage of virion production. Gastroenterology 128, 1056–1066.

Durantel, D., Zoulim, F., 2007. Going towards more relevant cell culture models to study the in vitro replication of serum-derived hepatitis C virus and virus/host cell interactions? J. Hepatol. 46, 1–5.

Eldar, A., Elowitz, M.B., 2010. Functional roles for noise in genetic circuits. Nature 467, 167–173.

El-Hage, N., Luo, G., 2003. Replication of hepatitis C virus RNA occurs in a membrane-bound replication complex containing nonstructural viral proteins and

RNA. J. General. Virol. 84, 2761–2769.
EM Agency, 2014. Olysio, INN-Simeprevir. European Medicines Agency.
Gale, M., Foy, E.M., 2005. Evasion of intracellular host defence by hepatitis C virus. Nature 436, 939–945.
Gandhi, S.J., Zenklusen, D., Lionnet, T., Singer, R.H., 2011. Transcription of functionally related constitutive genes is not coordinated. Nat. Struct. Mol. Biol. 18, 27–34.
Garaigorta, U., Chisari, F.V., 2009. Hepatitis C virus blocks interferon effector function by inducing protein kinase R phosphorylation. Cell Host Microbe 6, 513–522.
Garber, K., 2011. Hepatitis C: move over interferon. Nat. Biotechnol. 29, 963–966.
Golding, I., Paulsson, J., Zawilski, S.M., Cox, E.C., 2005. Real-time kinetics of gene activity in individual bacteria. Cell 123, 1025–1036.
Gosert, R., Egger, D., Lohmann, V., Bartenschlager, R., Blum, H.E., Bienz, K., Moradpour, D., 2003. Identification of the hepatitis C virus RNA replication complex in Huh-7 cells harboring subgenomic replicons. J. Virol. 77, 5487–5492.
Guedj, J., Dahari, H., Uprichard, S.L., Perelson, A.S., 2013. The rapid viral decline with the HCV NS5A inhibitor daclatasvir reveals a dual mode of action and leads to a new HCV half-life estimate. Expert Rev. Gastroenterol. Hepatol. 7, 397–399.
Guedj, J., Pang, P.S., Denning, J., Rodriguez-Torres, M., Lawitz, E., Symonds, W., Perelson, A.S., 2014. Analysis of hepatitis C viral kinetics during administration of two nucleotide analogues: sofosbuvir (GS-7977) and GS-0938. Antivir. Ther. 19, 211–220.
Guedj, J., Dahari, H., Rong, L., Sansone, N.D., Nettles, R.E., Cotler, S.J., Layden, T.J., Uprichard, S.L., Perelson, A.S., 2013. Modeling shows that the NS5A inhibitor daclatasvir has two modes of action and yields a shorter estimate of the hepatitis C virus half-life. Proc. Natl. Acad. Sci. 110, 3991–3996.
Guidotti, L.G., Chisari, F.V., 2006. Immunobiology and pathogenesis of viral hepatitis. Annu. Rev. Pathol. 1, 23–61.
Gustafsson, M.G.L., Shao, L., Carlton, P.M., Wang, C.J.R., Golubovskaya, I.N., Cande, W. Z., Agard, D.A., Sedat, J.W., 2008. Three-dimensional resolution doubling in wide-field fluorescence microscopy by structured illumination. Biophys. J. 94, 4957–4970.
Health AGDo, 2014. AusPAR: sofosbuvir. Australian Government Department of Health,.
Heim, M.H., Moradpour, D., Blum, H.E., 1999. Expression of Hepatitis C Virus Proteins Inhibits Signal Transduction through the Jak-STAT Pathway. J. Virol. 73, 8469–8475.
Holmberg, S.D., Spradling, P.R., Moorman, A.C., Denniston, M.M., 2013. Hepatitis C in the United States. N. Engl. J. Med. 368, 1859–1861.
Horner, S.M., Gale, M., 2009. Intracellular innate immune cascades and interferon defenses that control hepatitis C virus. J. Interferon Cytokine Res. 29, 489–498.
Jones, C.T., Catanese, M.T., Law, L.M.J., Khetani, S.R., Syder, A.J., Ploss, A., Oh, T.S., Schoggins, J.W., MacDonald, M.R., Bhatia, S.N., Rice, C.M., 2010. Real-time imaging of hepatitis C virus infection using a fluorescent cell-based reporter system. Nat. Biotech. 28, 167–171.
Jouvenet, N., Simon, S.M., Bieniasz, P.D., 2009. Imaging the interaction of HIV-1 genomes and Gag during assembly of individual viral particles. Proc. Natl. Acad. Sci. 106, 19114–19119.
Kazakov, T., Yang, F., Ramanathan, H.N., Kohlway, A., Diamond, M.S., Lindenbach, B. D., 2015. Hepatitis C virus RNA replication depends on specific *Cis*- and *Trans* – acting activities of viral nonstructural proteins. Plos. Pathog. 11, e1004817.
Komurian-Pradel, F., Perret, M., Deiman, B., Sodoyer, M., Lotteau, V., Paranhos-Baccalà, G., André, P., 2004. Strand specific quantitative real-time PCR to study replication of hepatitis C virus genome. J. Virol. Methods 116, 103–106.
Kowdley, K.V., Gordon, S.C., Reddy, K.R., Rossaro, L., Bernstein, D.E., Lawitz, E., Shiffman, M.L., Schiff, E., Ghalib, R., Ryan, M., Rustgi, V., Chojkier, M., Herring, R., Di Bisceglie, A.M., Pockros, P.J., Subramanian, G.M., An, D., Svarovskaia, E., Hyland, R.H., Pang, P.S., Symonds, W.T., McHutchison, J.G., Muir, A.J., Pound, D., Fried, M.W., 2014. Ledipasvir and Sofosbuvir for 8 or 12 weeks for chronic HCV without cirrhosis. N. Engl. J. Med. 370, 1879–1888.
Lanford, R.E., Chavez, D., Chisari, F.V., Sureau, C., 1995. Lack of detection of negative-strand hepatitis C virus RNA in peripheral blood mononuclear cells and other extrahepatic tissues by the highly strand-specific rTth reverse transcriptase PCR. J. Virol. 69, 8079–8083.
Lee, C., Ma, H., Hang, J.Q., Leveque, V., Sklan, E.H., Elazar, M., Klumpp, K., Glenn, J. S., 2011. The hepatitis C virus NS5A inhibitor (BMS-790052) alters the subcellular localization of the NS5A non-structural viral protein. Virology 414, 10–18.
Lemon, S.M., 2010. Induction and evasion of innate antiviral responses by hepatitis C virus. J. Biol. Chem. 285, 22741–22747.
Li, K., Lemon, S.M., 2013. Innate immune responses in hepatitis C virus infection. Semin Immunopathol. 35, 53–72.
Li, Y., Yamane, D., Masaki, T., Lemon, S.M., 2015. The yin and yang of hepatitis C: synthesis and decay of hepatitis C. virus Rna. Nat. Rev. Micro 13, 544–558.
Liang, Y., Shilagard, T., Xiao, S.Y., Snyder, N., Lau, D., Cicalese, L., Weiss, H., Vargas, G., Lemon, S.M., 2009. Visualizing hepatitis C virus infections in human liver by two-photon microscopy. Gastroenterology 137, 1448–1458.
Lin, W., Kim, S.S., Yeung, E., Kamegaya, Y., Blackard, J.T., Kim, K.A., Holtzman, M.J., Chung, R.T., 2006. Hepatitis C virus core protein blocks interferon signaling by interaction with the STAT1 SH2 domain. J. Virol. 80, 9226–9235.
Lindenbach, B.D., Evans, M.J., Syder, A.J., Wölk, B., Tellinghuisen, T.L., Liu, C.C., Maruyama, T., Hynes, R.O., Burton, D.R., McKeating, J.A., Rice, C.M., 2005. Complete replication of hepatitis C virus in cell culture. Science 309, 623–626.
Lindenbach, B.D., Evans, M.J., Syder, A.J., Wolk, B., Tellinghuisen, T.L., Liu, C.C., Maruyama, T., Hynes, R.O., Burton, D.R., McKeating, J.A., Rice, C.M., 2005. Complete replication of hepatitis C virus in cell culture. Science 309, 623–626.
Lohmann, V., Körner, F., Koch, J.-O., Herian, U., Theilmann, L., Bartenschlager, R., 1999. Replication of subgenomic hepatitis C virus RNAS in a hepatoma cell line. Science 285, 110–113.
Marukian, S., Jones, C.T., Andrus, L., Evans, M.J., Ritola, K.D., Charles, E.D., Rice, C.M., Dustin, L.B., 2008. Cell culture–produced hepatitis C virus does not infect peripheral blood mononuclear cells. Hepatology 48, 1843–1850.
Marukian, S., Andrus, L., Sheahan, T.P., Jones, C.T., Charles, E.D., Ploss, A., Rice, C.M., Dustin, L.B., 2011. Hepatitis C virus induces interferon-lambda and interferon-stimulated genes in primary liver cultures. Hepatology 54, 1913–1923.
McGivern, D.R., Masaki, T., Williford, S., Ingravallo, P., Feng, Z., Lahser, F., Asante-Appiah, E., Neddermann, P., De Francesco, R., Howe, A.Y., Lemon, S.M., 2014. Kinetic analyses reveal potent and early blockade of hepatitis C virus assembly by NS5A inhibitors. Gastroenterology 147 453–462.e457.
McGuinness, P.H., Bishop, G.A., McCaughan, G.W., Trowbridge, R., Gowans, E.J., 1994. False detection of negative-strand hepatitis C virus RNA. Lancet 343, 551–552.
Mee, C.J., Grove, J., Harris, H.J., Hu, K., Balfe, P., McKeating, J.A., 2008. Effect of cell polarization on hepatitis C virus entry. J. Virol. 82, 461–470.
Metz, P., Reuter, A., Bender, S., Bartenschlager, R., 2013. Interferon-stimulated genes and their role in controlling hepatitis C virus. J. Hepatol. 59, 1331–1341.
Moradpour, D., Penin, F., Rice, C.M., 2007. Replication of hepatitis C virus. Nat. Rev. Micro 5, 453–463.
Mulligan, E.K., Germer, J.J., Arens, M.Q., D'Amore, K.L., Di Bisceglie, A., Ledeboer, N. A., Moser, M.J., Newman, A.C., O'Guin, A.K., Olivo, P.D., Podzorski, D.S., Vaughan, K.A., Yao, J.D., Elagin, S.A., Johnson, S.C., 2009. Detection and quantification of hepatitis C virus (HCV) by MultiCode-RTx real-time PCR targeting the HCV 3′ untranslated region. J. Clin. Microbiol. 47, 2635–2638.
Mutch, S.A., Fujimoto, B.S., Kuyper, C.L., Kuo, J.S., Bajjalieh, S.M., Chiu, D.T., 2007. Deconvolving single-molecule intensity distributions for quantitative microscopy measurements. Biophys. J. 92, 2926–2943.
Nakabayashi, H., Taketa, K., Miyano, K., Yamane, T., Sato, J., 1982. Growth of human hepatoma cell lines with differentiated functions in chemically defined medium. Cancer Res. 42, 3858–3863.
Neumann, A.U., Lam, N.P., Dahari, H., Gretch, D.R., Wiley, T.E., Layden, T.J., Perelson, A.S., 1998. Hepatitis C viral dynamics in vivo and the antiviral efficacy of interferon-α therapy. Science 282, 103–107.
Paul, D., Madan, V., Bartenschlager, R., 2014. Hepatitis C virus RNA replication and assembly: living on the fat of the land. Cell Host Microbe 16, 569–579.
Perelson, A.S., Guedj, J., 2015. Modelling hepatitis C therapy[mdash]predicting effects of treatment. Nat. Rev. Gastroenterol. Hepatol. 12, 437–445.
Pietschmann, T., Kaul, A., Koutsoudakis, G., Shavinskaya, A., Kallis, S., Steinmann, E., Abid, K., Negro, F., Dreux, M., Cosset, F.-L., Bartenschlager, R., 2006. Construction and characterization of infectious intragenotypic and intergenotypic hepatitis C virus chimeras. Proc. Natl. Acad. Sci. 103, 7408–7413.
Quinkert, D., Bartenschlager, R., Lohmann, V., 2005. Quantitative analysis of the hepatitis C virus replication complex. J. Virol. 79, 13594–13605.
Raj, A., van Oudenaarden, A., 2008. Nature, nurture, or chance: stochastic gene expression and its consequences. Cell 135, 216–226.
Raj, A., van Oudenaarden, A., 2009. Single-molecule approaches to stochastic gene expression. Annu. Rev. Biophys. 38, 255–270.
Raj, A., Rifkin, S.A., Andersen, E., van Oudenaarden, A., 2010. Variability in gene expression underlies incomplete penetrance. Nature 463, 913–918.
Raj, A., van den Bogaard, P., Rifkin, S.A., van Oudenaarden, A., Tyagi, S., 2008. Imaging individual mRNA molecules using multiple singly labeled probes. Nat. Methods 5, 877–879.
Revie, D., Salahuddin, S., 2011. Human cell types important for Hepatitis C Virus replication in vivo and in vitro. Old assertions and current evidence. Virology 8, 346.
Robertson, K.L., Verhoeven, A.B., Thach, D.C., Chang, E.L., 2010. Monitoring viral RNA in infected cells with LNA flow-FISH. RNA 16, 1679–1685.
Rong, L., Perelson, A.S., 2013. Mathematical analysis of multiscale models for hepatitis C virus dynamics under therapy with direct-acting antiviral agents. Math. Biosci. 245, 22–30.
Sadler, A.J., Williams, B.R.G., 2008. Interferon-inducible antiviral effectors. Nat. Rev. Immunol. 8, 559–568.
Sarasin-Filipowicz, M., Oakeley, E.J., Duong, F.H.T., Christen, V., Terracciano, L., Filipowicz, W., Heim, M.H., 2008. Interferon signaling and treatment outcome in chronic hepatitis C. Proc. Natl. Acad. Sci. 105, 7034–7039.
Schermelleh, L., Carlton, P.M., Haase, S., Shao, L., Winoto, L., Kner, P., Burke, B., Cardoso, M.C., Agard, D.A., Gustafsson, M.G.L., Leonhardt, H., Sedat, J.W., 2008. Subdiffraction multicolor imaging of the nuclear periphery with 3D structured illumination microscopy. Science 320, 1332–1336.
Schoggins, J.W., Wilson, S.J., Panis, M., Murphy, M.Y., Jones, C.T., Bieniasz, P., Rice, C. M., 2011. A diverse range of gene products are effectors of the type I interferon antiviral response. Nature 472, 481–485.
Schwartz, Trehan, Andrus, L., Sheahan, T.P., Ploss, A., Duncan, S.A., Rice, C.M., Bhatia, S.N., 2012. Modeling hepatitis C virus infection using human induced plur-ipotent stem cells. Proc. Natl. Acad. Sci.
Schwartz, R., Trehan, K., Andrus, L., Sheahan, T.P., Ploss, A., Duncan, S.A., Rice, C.M., Bhatia, S.N., 2012. Modeling hepatitis C virus infection using human induced pluripotent stem cells. Proc. Natl. Acad. Sci.
Shaffer, S.M., Wu, M.-T., Levesque, M.J., Raj, A., 2013. Turbo FISH: a method for rapid single molecule RNA FISH. Plos. One 8, e75120.
Shalek, A.K., Satija, R., Adiconis, X., Gertner, R.S., Gaublomme, J.T., Raychowdhury, R., Schwartz, S., Yosef, N., Malboeuf, C., Lu, D., Trombetta, J.T., Gennert, D., Gnirke, A., Goren, A., Hacohen, N., Levin, J.Z., Park, H., Regev, A., 2013. Single-cell

transcriptomics reveals bimodality in expression and splicing in immune cells. Nature 498, 236–240.
Shepard, C.W., Finelli, L., Alter, M.J., 2005. Global epidemiology of hepatitis C virus infection. Lancet Infect. Dis. 5, 558–567.
Shimakami, T., Yamane, D., Jangra, R.K., Kempf, B.J., Spaniel, C., Barton, D.J., Lemon, S.M., 2012. Stabilization of hepatitis C virus RNA by an Ago2–miR-122 complex. Proc. Natl. Acad. Sci. U.S.A. 109, 941–946.
Shulla, A., Randall, G., 2015. Spatiotemporal analysis of hepatitis C virus infection. Plos Pathog. 11, e1004758.
Si-Tayeb, K., Noto, F.K., Nagaoka, M., Li, J., Battle, M.A., Duris, C., North, P.E., Dalton, S., Duncan, S.A., 2010. Highly efficient generation of human hepatocyte–like cells from induced pluripotent stem cells. Hepatology 51, 297–305.
Snijder, B., Pelkmans, L., 2011. Origins of regulated cell-to-cell variability. Nat. Rev. Mol. Cell Biol. 12, 119–125.
Snijder, B., Sacher, R., Ramo, P., Damm, E.-M., Liberali, P., Pelkmans, L., 2009. Population context determines cell-to-cell variability in endocytosis and virus infection. Nature 461, 520–523.
So, L.-h., Ghosh, A., Zong, C., Sepulveda, L.A., Segev, R., Golding, I., 2011. General properties of transcriptional time series in Escherichia coli. Nat. Genet 43, 554–560.
Sumpter, R., Loo, Y.-M., Foy, E., Li, K., Yoneyama, M., Fujita, T., Lemon, S.M., Gale, M., 2005. Regulating intracellular antiviral defense and permissiveness to hepatitis C virus RNA replication through a cellular RNA helicase, RIG-I. J. Virol. 79, 2689–2699.
Tan, R.Z., van Oudenaarden, A., 2010. Transcript counting in single cells reveals dynamics of rDNA transcription. Mol. Syst. Biol. 6.
Theofilopoulos, A.N., Baccala, R., Beutler, B., Kono, D.H., 2005. Type I interferons (α/β) in immunity and autoimmunity. Annu. Rev. Immunol. 23, 307–335.
Tscherne, D.M., Evans, M.J., von Hahn, T., Jones, C.T., Stamataki, Z., McKeating, J.A., Lindenbach, B.D., Rice, C.M., 2007. Superinfection exclusion in cells infected with hepatitis C virus. J. Virol. 81, 3693–3703.
Vargas, D.Y., Raj, A., Marras, S.A.E., Kramer, F.R., Tyagi, S., 2005. Mechanism of mRNA transport in the nucleus. Proc. Natl. Acad. Sci. USA 102, 17008–17013.
Walters, K.-A., Syder, A.J., Lederer, S.L., Diamond, D.L., Paeper, B., Rice, C.M., Katze, M.G., 2009. Genomic analysis reveals a potential role for cell cycle perturbation in HCV-mediated apoptosis of cultured hepatocytes. Plos Pathog. 5, e1000269.
Wieland, S., Makowska, Z., Campana, B., Calabrese, D., Dill, M.T., Chung, J., Chisari, F. V., Heim, M.H., 2014. Simultaneous detection of hepatitis C virus and interferon stimulated gene expression in infected human liver. Hepatology 59, 2121–2130.
Wong, M.T., Chen, S.S., 2014. Emerging roles of interferon-stimulated genes in the innate immune response to hepatitis C virus infection. Cell Mol. Immunol.
Yang, D., Liu, N., Zuo, C., Lei, S., Wu, X., Zhou, F., Liu, C., Zhu, H., 2011. Innate host response in primary human hepatocytes with hepatitis C virus infection. Plos One 6, e27552.